Journal of Inorganic Biochemistry 213 (2020) 111264

Contents lists available at ScienceDirect

Journal of Inorganic Biochemistry

journal homepage: www.elsevier.com/locate/jinorgbio

Effect of coordination dissymmetry on the catalytic activity of manganese catalase mimics

Ripul Mehrotra [a,1], Micaela Richezzi [a], Claudia Palopoli [a], Christelle Hureau [b], Sandra R. Signorella [a,*]

[a] IQUIR (Instituto de Quimica Rosario), Consejo Nacional de Investigaciones Cientificas y Tecnicas (CONICET), Facultad de Ciencias Bioquimicas y Farmaceuticas, Universidad Nacional de Rosario, Suipacha 531, S2002LRK Rosario, Argentina

[b] CNRS, LCC (Laboratoire de Chimie de Coordination) and UPS, INPT, LCC, Université de Toulouse, 205 route de Narbonne, F-31077 Toulouse, France

ARTICLE INFO

Keywords:
Biomimics
diMn complexes
Unsymmetrical ligands
CAT activity
Mechanism
Spectroscopy

ABSTRACT

Two mixed-valence Mn(II)Mn(III) complexes, $[Mn_2L^1(OAc)_2(H_2O)]BPh_4{\cdot}2.5H_2O$ and $[Mn_2L^2(OAc)_2]{\cdot}4H_2O$, obtained with unsymmetrical N_4O_2-hexadentate $L^{1(2-)}$ (H_2L^1 = 2-(*N*,*N*-bis(2-(pyridylmethyl)aminomethyl)-6-(N-(2-hydroxybenzyl)benzylaminomethyl)-4-methylphenol) and N_4O_3-heptadentate $L^{2(3-)}$ (NaH_2L^2 = 2-(*N*,*N*-bis(2-(pyridylmethyl)aminomethyl)-6-(N′-(2-hydroxybenzyl)(carboxymethyl)aminomethyl)-4-methylphenol sodium salt) ligands, have been prepared and characterized. Both complexes share a μ-phenolate-bis(μ-acetate)Mn(II)Mn(III) core and N_3O_3-coordination sphere around the Mn(II) ion, but differ in the donor groups surrounding Mn(III) (NO_4(solvent) and NO_5). In non-protic solvents, these two complexes are able to disproportionate at least 3600 equiv. of H_2O_2 without significant decomposition, with first-order dependence on catalyst and saturation kinetics on $[H_2O_2]$. Spectroscopic monitoring of the reaction mixtures revealed the two complexes disproportionate H_2O_2 employing a different redox cycle, with retention of dinuclearity. The higher catalytic efficiency of $[Mn_2L^2(OAc)_2]$ was rationalized in terms of the larger labilizing effect of the heptadentate ligand that favors the acetate-shift and the replacement of the non-coordinating benzyl arm of L^1 by a carboxylate arm in L^2 which facilitates the formation of the catalyst-H_2O_2 adduct, placing $[Mn_2L^2(OAc)_2]$ as the most efficient among the phenolate-bridged diMn catalysts based on the k_{cat}/K_M criterion.

1. Introduction

H_2O_2 is a by-product of aerobic metabolism in respiratory and photosynthetic electron-transport chains and a product of enzymatic activity [1]. Excess of H_2O_2 and hydroxyl radical, its decomposition product formed via a Fenton-type reaction, are harmful for almost all cell components. Thus, the rapid and efficient removal of H_2O_2 is essential to all aerobically living prokaryotic and eukaryotic cells. Catalase (CAT) enzymes are present in most aerobic forms of life and are responsible for the decomposition of H_2O_2 into molecular oxygen and water [2]. In many pathological conditions and diseases, including cancer, neurological disorders, atherosclerosis, hypertension, ischemia/perfusion, diabetes, etc., the endogenous antioxidant systems can be overwhelmed. Administration of exogenous enzymes for the treatment of oxidative stress is limited by their short half-life, antigenicity, high cost, and large sizes that disable the enzymes to cross the cell membranes [3,4]. Therefore, low molecular weight enzyme mimics constitute an alternative to overcome these limitations [5–7], some of which have proven to protect cells from oxidative damage in animal models [8].

Manganese catalases (MnCAT) contain two Mn ions at their active site and catalyze the disproportionation of H_2O_2 through a $Mn(II)_2$ and $Mn(III)_2$ redox cycle [9–11]. The two metal ions of the diMn active site are triply bridged through a $\mu_{1,3}$-carboxylate of a glutamate residue and two solvent-derived bridges (either aqua, hydroxo, or oxo ligands) and terminally bound to His and Glu [12,13]. Both Mn subsites are six-coordinate but only one of them is bound to a labile water molecule where initial substrate binding is presumed to occur. This coordination dissymmetry around the two metal ions could be essential for catalysis. However, most diMn complexes tested as MnCAT mimics have been prepared with symmetrical dinucleating ligands with a central alcoholate or phenolate group that afford synthetic models with identical

* Corresponding author.
E-mail address: signorella@iquir-conicet.gov.ar (S.R. Signorella).
[1] Present address: Department of chemistry, Govt. College Chhapara, District-Seoni, Madhya Pradesh, India.

https://doi.org/10.1016/j.jinorgbio.2020.111264
Received 2 August 2020; Received in revised form 9 September 2020; Accepted 21 September 2020
Available online 28 September 2020

environment around the two metal centers [14–18], while only a few ones were made from unsymmetrical ligands [19–21].

With the aim of reproducing the singularities of the biosite, we report here the synthesis, properties and CAT activity of two diMn complexes obtained with unsymmetrical ligands bearing a central phenolate group: 2-(*N*,*N*-bis(2-(pyridylmethyl)aminomethyl)-6-(N-(2-hydroxybenzyl) benzylaminomethyl)-4-methylphenol (H_2L^1) and 2-(*N*,*N*-bis(2-(pyridylmethyl)aminomethyl)-6-(N′-(2-hydroxybenzyl)(carboxymethyl) aminomethyl)-4-methylphenol sodium salt (NaH_2L^2), and compare the kinetic results to other diMn mimics. These ligands offer two different coordination compartments to build bimetallic sites with different environment around each metal center and will be used for assessing the influence of the ligand dissymmetry on the CAT activity of the diMn complexes.

2. Experimental part

2.1. Synthesis of the ligands

The secondary amines, bis(2-pyridylmethyl)amine, N-(2-hydroxybenzyl)benzylamine and N-(2-hydroxybenzyl)glycine chlorohydrate were prepared as reported previously [22–24]. Intermediates (6-methyl-2-phenyl-2,4-dihydro-1,3-benzodioxin-8-yl)methanol (**1**), 8-(bromomethyl)-6-methyl-2-phenyl-2,4-dihydro-1,3-benzodioxine (**2**), 8-(bis(2-pyridylmethyl)aminomethyl)-6-methyl-2-phenyl-2,4-dihydro-1,3-benzodioxine (**3**), 2-(*N*,*N*-bis(2-(pyridylmethyl)aminomethyl)-6-(hydroxymethyl)-4-methylphenol (**4**) and 2-(*N*,*N*-bis(2-(pyridylmethyl) aminomethyl)-6-(chloromethyl)-4-methylphenol (**5**), were synthesized following procedures described in references [23, 25–27]. Synthetic details for the obtention of these compounds are described in the supplementary information.

2.1.1. 2-(N,N-Bis(2-(pyridylmethyl)aminomethyl)-6-(N-(2-hydroxybenzyl)benzylaminomethyl)-4-methylphenol (***H_2L^1***)

To a solution of **5** (533.6 mg, 1.45 mmoL) and *N*-(2-hydroxybenzyl) benzylamine (309 mg, 1.45 mmoL) dissolved in THF (15 mL), 200 μL of Et_3N were added and left with stirring at room temperature for 6 days. The solid formed was removed by filtration. After evaporation of THF, a red yellow oil was obtained. This oil was further dissolved in 5 mL CH_2Cl_2 and washed with phosphate buffer (pH 7.0). The organic layers were collected, dried over Na_2SO_4 and filtered. After solvent evaporation the solid product was obtained. Yield: 380.2 mg, 48.1%. ^{1}H NMR spectrum (δ, $CDCl_3$, ppm): 8.56 (d, 2H, Ar-H_{py}); 7.60–7.54 (td, 2H, Ar—H); 7.45 (d, 1H, Ar—H); 7.36–7.31 (m, 5H, Ar—H); 7.28–7.24 (m, 1H, Ar—H); 7.16–7.12 (t, 2H, Ar—H); 7.10–7.09 (m,1H, Ar—H); 6.99–6.97 (d, 1H, Ar—H); 6.91 (s, 1H, Ar—H); 6.80–6.70 (t, 2H, Ar—H); 6.74–6.71 (dd, 1H, Ar-H); 3.86 (s, 4H, Ar_{py}-CH_2-N); 3.79 (s, 2H, –CH_2); 3.74 (s, 2H, –CH_2); 3.72 (s, 2H, –CH_2); 3.68 (s, 2H, –CH_2); and 2.22 (s, 3H, CH_3). ^{13}C NMR spectrum (δ, $CDCl_3$, ppm): 158.23, 157.7, 154.15, 148.92, 136.73, 131.42, 130.44, 129.71, 128.90, 128.41, 128.30, 127.46, 127.24, 126.55, 123.27, 122.67, 122.18, 118.82, 115.98, 59.16, 57.93, 57.13, 56.70, and 20.43. Significant IR bands (ATR, ν cm^{-1}): 3356, 2914, 1589, 1454, 1433, 1357, 746, and 696.

2.1.2. 2-(N,N-Bis(2-(pyridylmethyl)aminomethyl)-6-(N′-(2-hydroxybenzyl)(carboxymethyl) aminomethyl)-4-methylphenol sodium salt (***NaH_2L^2***)

A solution of **5** (1.36 mmol, 500 mg) in 15 mL THF was added to N-(2-hydroxybenzyl)glycine chlorohydrate (296 mg, 1.36 mmol) in 5 mL of 0.55 M NaOH aqueous solution. The mixture was left with stirring for 48 h. THF was removed under vacuum and 20 mL CH_2Cl_2 added to the aqueous residue. The organic layer was separated and washed with phosphate buffer of pH 7.0 (3 × 10 mL), dried over Na_2SO_4 and filtered. After concentration of the filtrate, hexane was added and a yellow solid formed when cooled at 4 °C. Recrystallization from 2:8 $CHCl_3$:hexane mixture afforded a bright yellow solid. Yield: 139 mg (19.2%). ^{1}H NMR spectrum (δ, MeOD, ppm): 8.49 (d, 1H, Ar-H_{Py}), 8.38 (d, 1H, Ar-H_{Py}), 7.69 (dt, 1H, Ar—H), 7.61 (dt, 1H, Ar—H), 7.39 (m, 2H, Ar—H), 7.23 (m, 2H, Ar—H), 7.02 (m, 2H, Ar—H), 6.85 (m, 2H, Ar-H), 6.78 (s, 2H, Ar-H), 3.84 (s, 4H, Ar_{py}-CH_2-N), 3.74 (s, 2H, -CH_2-), 3.72 (s, 2H, CH_2), 3.68 (s, 2H, CH_2), 3.56 (s, 2H, -CH_2-CO_2), and 2.23 (s, 3H, CH_3). ^{13}C NMR spectrum (δ, MeOD, ppm): 168.93, 157.96, 157.92, 156.45, 154.03, 148.22, 148.01, 137.44, 137.22, 132.73, 131.75, 131.17, 128.29, 128.06, 127.57, 123.68, 123.51, 123.45, 123.18, 122.44, 122.40, 119.62, 115.12, 59.34, 58.64, 58.28, 58.12, 56.40, 55.90, 54.85, 54.32, and 18.94. Significant IR bands (ATR, ν cm^{-1}): 3420, 2075, 3010, 2917, 2847, 1636, 1591, 1435, 1381, 862, and 760.

2.2. Synthesis of complexes

2.2.1. Complex [$Mn_2L^1(OAc)_2(H_2O)$]BPh_4·2.5H_2O (**6**·2.5H_2O)

A solution of H_2L^1 (113.2 mg, 0.208 mmoL) in CH_3OH (2 mL) was added to a methanolic solution of manganese(II) acetate tetrahydrate (102 mg, 0.416 mmoL) and left with stirring at room temperature for 2 h. The addition of a methanolic solution (2 mL) of $NaBPh_4$ (71.1 mg) caused the formation of a brown precipitate, which was collected by filtration, washed with methanol and hexane and dried under vacuum. Yield: 0.1920 g (0.167 mmol), 80.0%. Thin layer chromatography (TLC) of **6** using different mobile phases (in different ratios) and three different stationary phases (silica, alumina and cellulose) showed only one spot. Anal. calcd. for $BC_{63}H_{62}Mn_2N_4O_7$·2.5H_2O: C 65.6, H 5.9, Mn 9.5, and N 4.9, %; Found: C 65.5, H 5.6, Mn 9.2, and N 5.3%. Molar conductivity (CH_3OH) = 129 Ω^{-1} cm^2 mol^{-1}. UV–vis, λ_{max} nm (ε M^{-1} cm^{-1}) in *N*,*N*-dimethylformamide (DMF): 275 (20800), 365 (4168), 450 (sh), and 608 (264). Significant IR bands (KBr, ν cm^{-1}): 3445 (broad), 3055, 3030, 2920, 2853, 1625, 1595, 1560, 1431, 864, 734, 705, 644, and 611. The content of 2.5 molecules of non-coordinated water per complex molecule was confirmed by thermogravimetric analysis of the complex which showed 3.9% mass loss below 120 °C.

2.2.2. Complex [$Mn_2L^2(OAc)_2$]·4H_2O (**7**·4H_2O)

A solution of NaH_2L^2 (100 mg, 0.187 mmol) in 8 mL CH_3OH was mixed with a solution of $Mn(OAc)_2$·4H_2O (92 mg, 0.378 mmol) in 2 mL CH_3OH, and the red brown mixture was left with stirring for 3 h. Then the volume was reduced to 2 mL under vacuum, 10 mL ethyl ether were added, and the mixture cooled to 4 °C. After 3 h, the formed brown precipitate was filtered off, washed with cool CH_3OH and ether and dried under vacuum. Yield: 108 mg, 78.3%. TLC of **7** using different mobile phases (in different ratios) and three different stationary phases (silica, alumina and cellulose) showed only one spot. Anal. calcd. for $C_{34}H_{35}Mn_2N_4O_8$·4H_2O: C 50.4, H 5.4, Mn 13.6, and N 6.9, %; Found: C 50.1, H 5.1, Mn 13.7, and N 6.7%. UV–vis, λ_{max} nm (ε M^{-1} cm^{-1}) in DMF: 279 (21350), 345 (4105), 462 (1665), and 694 (293). Significant IR bands (KBr, ν cm^{-1}): 3435 (broad), 3065, 3032, 3004, 2921, 2859, 1624, 1590, 1574, 1422, 806, 761, 654, and 630. The content of 4 molecules of non-coordinated water per complex molecule was confirmed by thermogravimetric analysis of the complex which showed 8.9% mass loss below 120 °C.

2.3. Analytical and physical measurements

Infrared spectra were recorded on a Perkin-Elmer Spectrum One FTIR spectrophotometer in the 4000–400 cm^{-1} range. UV–visible spectra were recorded on a Jasco V-550 spectrophotometer, with thermostated cell compartments. Metal content was determined with an Inductively coupled plasma mass spectrometer (ICP-MS) Perkin Elmer NexION 350×. Electron Paramagnetic Resonance (EPR) spectra were obtained at 115 K on an Elexsys E 500 Bruker spectrometer, operating at a microwave frequency of approximately 9.5 GHz. Thermogravimetric analysis (TGA) measurements were conducted on a Perkin-Elmer Diamond TG/DTA Instrument. The compound was heated at the rate of 10 °C/min between RT and 800 °C. Conductivity measurements were

performed using a Horiba F-54 BW conductivity meter, on 1.0 mM solutions of the complexes in methanol. Electrospray ionization (ESI) mass spectra were obtained with a Thermo Scientific LCQ Fleet. The solutions for electrospray were prepared from solutions of complex or reaction mixtures diluted with acetonitrile to a final $\sim 10^{-5}$ M concentration. ^{1}H NMR spectra were recorded on a Bruker AC 300 NMR spectrometer at ambient probe temperature (ca. 25 °C). Chemical shifts (in ppm) are referenced to tetramethylsilane and paramagnetic NMR spectra were acquired employing superWEFT sequence, with acquisition time of 50 ms. The electrochemical experiments were performed with a computer-controlled Princeton Applied Research potentiostat, VERSASTAT II model, with the 270/250 Research Electrochemistry Software. Studies were carried out under Ar, in N,N-dimethylformamide (DMF) solution using 0.1 M Bu_4NPF_6 as a supporting electrolyte and $\approx 10^{-3}$ M of the complexes. The working electrode was a glassy carbon disk, and the reference electrode was a calomel electrode isolated in a fritted bridged with a Pt wire as the auxiliary electrode. All potentials are referred to the saturated calomel electrode (SCE). Under these conditions, *E*(ferrocene/ferrocenium) = 474 mV, in DMF.

2.4. Evaluation of CAT activity

Reaction rates were determined by volumetric measurement of the O_2 evolved after addition of excess of H_2O_2 to a DMF solution of the complex. A round-bottom flask with a rubber septum, containing the degassed solution of the complex, was thermostated at 25 °C and connected to a gas-measuring burette (precision of 0.1 mL). Previously thermostated H_2O_2 was injected through the septum to the stirred complex solution, and the evolved O_2 was measured with the burette. The initial reaction rates were obtained by fitting the $[O_2]$ versus time data to a polynomial expression and calculating the slope of the tangent at time zero. Each rate constant reported here represents the mean value of multiple determinations that fall within ±5%. All experiments were carried out at 25 °C. Blanc experiments performed with 100 mM H_2O_2 in DMF without the catalyst showed no decomposition after 1 h.

3. Results and discussion

3.1. Synthesis and characterization of complexes 6 and 7

The synthesis of the unsymmetrical ligands H_2L^1 and NaH_2L^2 is shown in Scheme 1.

The key step in the synthesis for introduction of dissymmetry is the formation of the cyclic acetal **1** to protect one of the terminal hydroxymethyl groups of the starting 2,6-bis(hydroxymethyl)-4-methylphenol [25]. Next, bromination and alkylation of bis-2-picolylamine afforded the N_3-branch. Acid hydrolysis of the acetal, followed by chlorination and subsequent alkylation of a second amine bearing terminal benzyl/phenol or carboxylate/phenol groups afforded the N_4O_2-hexadentate (H_2L^1) and N_4O_3-heptadentate (H_2NaL^2) ligand, respectively.

Dimanganese complexes **6** and **7** were prepared from 1:2 mixtures of the corresponding ligand and $Mn(OAc)_2{\cdot}4H_2O$ in methanol. Acetate facilitates the deprotonation of the ligand for coordination to the metal [28] and complexation occurs immediately after mixing, as evidenced

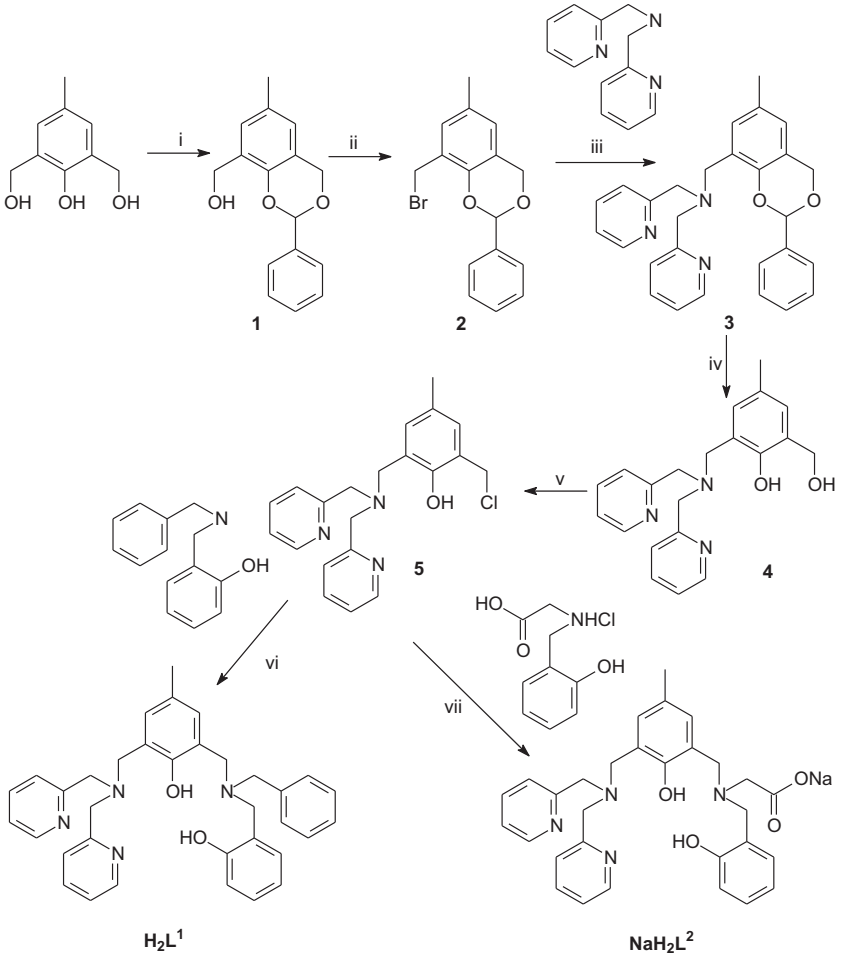

Scheme 1. Synthesis of unsymmetrical ligands. (i) $PhCH(OMe)_2$, p-$MeC_6H_4SO_3H$, DMF, 50 °C; (ii) CBr_4, PPh_3, DMF; (iii) NaH, CH_2Cl_2; (iv) HCl, THF, 0 °C; (v) Cl_2SO, 35 °C; (vi) Et_3N, THF; (vii) NaOH, THF

by the change of color of the reaction mixture from pale yellow to brown. Complex **6** was precipitated as a brown solid from the reaction mixture upon addition of the bulky BPh_4^-, while complex **7** separated from the solution as a brown solid after addition of ether at 4 °C.

The IR spectra of powdered **6** and **7** (Fig. S1) exhibit strong phenolate and pyridyl ring absorptions between 1625 and 1575 cm^{-1} as well as absorption bands at 1560–1574 cm^{-1} and 1431–1422 cm^{-1} attributable to the antisymmetrical and symmetrical stretching vibrations of carboxylate groups. For **6**, the three bands at 611, 705 and 734 cm^{-1} together with a strong and sharp stretching band at ~3055 cm^{-1} can be assigned to non-coordinated BPh_4^- counter anion, in agreement with its molecular structure. In line with the loss of H_2O evidenced by the thermogravimetric analysis, the two compounds display a broad band at ≈3440 cm^{-1} assigned to water molecules.

ESI-mass spectra of complexes **6** and **7** in CH_3CN (Fig. 1(a)) confirmed their chemical composition as well as retention of their nuclearity in solution. For complex **6**, the parent peak is observed at *m/z* = 811.2 in the positive mode ESI-mass spectra and originates from the $[Mn_2L^1(OAc)_2(CH_3CN)]^+$ monocation. Other peaks generated during the electrospray correspond to the exchange of AcO^- by HCO_2^- ($[Mn_2L^1(OAc)(HCO_2)]^+$, *m/z* = 757.2) and the loss of $Mn(OAc)_2$ ($[MnL^1H]^+$, *m/z* = 598.2). Complex **7** affords a mass spectrum with the major peak at *m/z* = 755.1 ($[Mn_2L^2(OAc)_2(H_2O)]^+$) and two minor peaks that can be assigned to $[Mn_2L^2(OAc)]^+$ at *m/z* = 678.1 and $[MnL^2Na]^+$ at *m/z* = 587.1. The isotopic patterns of these peaks match very well their simulated spectra. In addition, negative ion ESI-mass spectrum of complex **6** shows only one peak at *m/z* = 319 corresponding to BPh_4^- anion, in agreement with the molar conductivity of 129 Ω^{-1} cm^2 mol^{-1} for **6** in methanol, a value expected for a complex that behaves as a 1:1 electrolyte in solution.

Fig. 1(b) illustrates the X-band EPR spectra of the two powdered complexes at 120 K. These spectra exhibit two features, one around $g = 2$ which dominates the spectra and a low-field component at $g = 5$ for **6** and 6.8 for **7**, which can be associated with spin transitions in $S > ½$ spin states of the weakly coupled phenolate-bridged Mn(II)Mn(III) center, as already observed for other Mn(II)Mn(III) complexes [29–30].

The electronic spectra of complexes **6** and **7** (Fig. 1(c)) recorded in DMF exhibit an intense absorption at 275 and 279 nm, respectively, assigned to π-π* transitions within the ligands, and two moderately intense bands in the region 330–550 nm attributed to ligand-to-metal charge transfer (*LMCT*) transitions from pπ orbital of phenolate (either bridging or terminal phenolate) to partially filled dσ* and dπ* orbitals of Mn(III) [17,19,31,32] with an additional contribution of carboxylate-to-Mn(III) *CT* on the lower energy band [33]. The low intensity broad band observed around 608 nm (ε = 265 M^{-1} cm^{-1}) for **6** and at 698 nm (ε = 294 M^{-1} cm^{-1}) for **7**, corresponds to d-d transitions of the Mn(III) ion in agreement with reported values for related Mn(II)Mn(III) complexes [31,34]. The red shift of the d-d band can be interpreted in terms of the effect of the axial or equatorial position of the terminal phenolate group in the two complexes (Fig. 2). The more distant binding of phenolate to the Mn(III) ion on the elongation Jean-Teller axis weakens the metal-phO_{ax} bond reducing the d-d energy gap and this can account for red

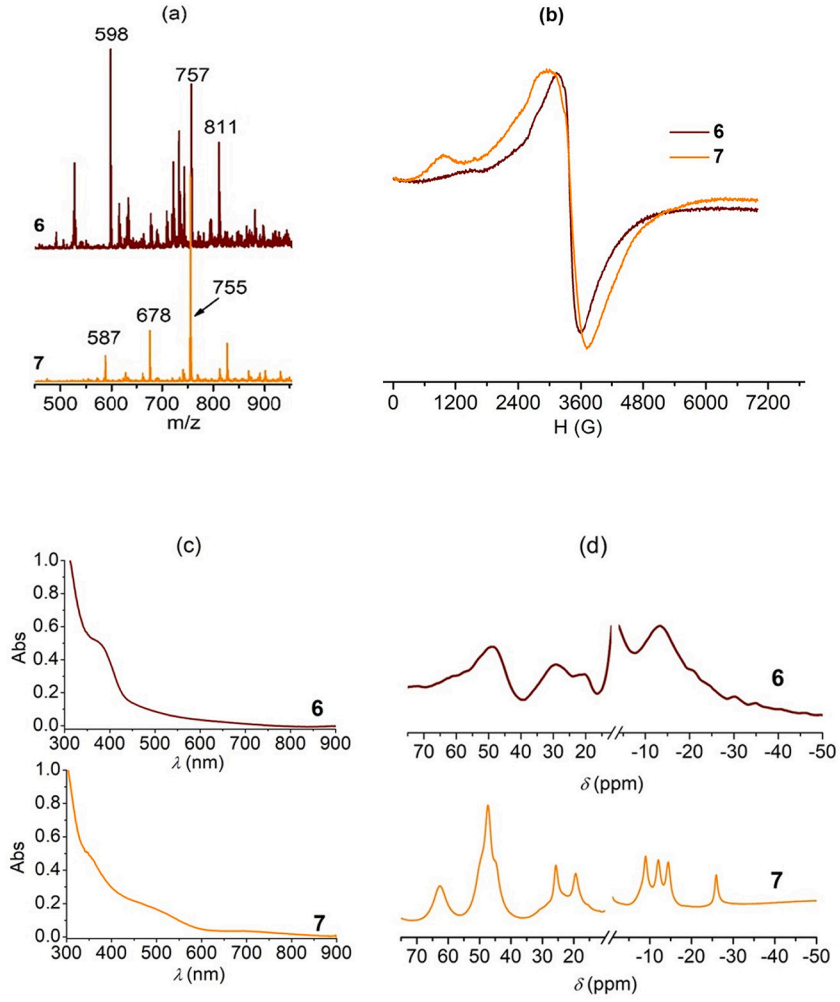

Fig. 1. (a) ESI-mass spectra of **6** and **7**, in MeCN, positive mode. (b) EPR spectra of solid complexes, ν = 9.5 GHz, T = 120 K, microwave power = 0.5 mW. (c) Electronic spectra of **6** and **7** in DMF. [complex] = 0.125 mM; l = 1 cm. (d) ^1H NMR spectra of **6** in $DCCl_3$ and **7** in CD_3OD. [complex] = 15 mM.

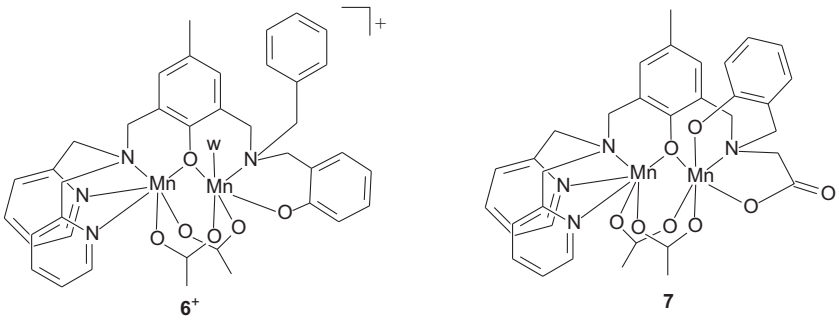

Fig. 2. Schematic structure formulas of the diMn complexes under study. w = water.

shift of this band in the spectrum of **7** relative to **6** [35]. The contribution of other electronic transitions disable direct comparison of the energy of the phenolate-to-Mn(III) *CT* bands. Electronic spectra of the two complexes registered at different times after preparing the DMF solutions (up to 24 h), showed identical molar absorption coefficients, indicating that both are stable in this solvent.

The ^{1}H NMR spectrum of solutions of **6** and **7** (Fig. 1(d)) show resonances outside the diamagnetic region spanning from 70 to −30 ppm. For the two complexes the signals appear in the same spectral region according to a weak magnetic coupling between the metal ions; however, resonances are much narrower for **7** as a consequence of the different spatial arrangement of the ligands in the two compounds. For **6**, the spectral pattern comprises a set of broad signals at 60, 48, 29, 20 and −13 ppm (linewidth in the range of 2500 to 3500 Hz) ascribed to phenolate/pyridine ring protons with even broader peaks of methylene protons spanning the full spectral range [36]. For **7**, the spectrum is better resolved showing intense resonances at 62, 49, 47 and 45 ppm ($w_{1/2}$ = 1200 Hz), and relatively sharp resonances at 26, 19, −9, −12 and −14.5 ppm ($w_{1/2}$ = 600 Hz), and −26 ppm ($w_{1/2}$ = 300 Hz). These peaks can be attributed to phenol and pyridine ring protons shifted down- and upfield as a consequence of spin-delocalization and dipolar effects, the last playing an important role in this kind of mixed-valence Mn(II)Mn(III) complexes [37].

The 1–10 ppm region of the ^{1}H NMR spectra of the complexes (Fig. S2) show peaks belonging to the solvent, and BPh_4^- in the case of complex **6**, without traces of the ligand, indicating the compounds are stable towards metal dissociation. Besides, no signal attributable to terminally coordinated acetate (broad signal at around 1.9 ppm [38]) is observed, which suggests that the most plausible structure for the two complexes in solution contains two bridging acetate ligands as shown in Fig. 2.

3.2. Electrochemical studies

The electrochemical properties of complexes **6** and **7** were investigated by cyclic voltammetry in DMF solutions containing 0.1 M Bu_4NPF_6 (Fig. S3). The two complexes exhibit one quasi-reversible reduction wave at $E_{1/2}$ = 0.058 V (**6**) and −0.164 V (**7**). Linear voltammetry confirmed that these waves correspond to reduction processes. $W_{1/2}$ values of 0.12 V for **6** and 0.13 V for **7** in the square-wave voltammetry (SWV) experiments (Fig. S3(a–b)) suggest that these reductions correspond to one-electron processes and may be attributed to the Mn(II)Mn(III)/Mn(II)Mn(II) redox couple.

On the oxidative side, **6** shows two anodic waves at E_{pa1} = 0.44 V (from deconvolution of the SWV wave) and $E_{1/2(2)}$ = 0.54 V vs *SCE* (ΔE_p = 0.14 V) (Fig. S3(c)). These two one-electron oxidation processes might correspond to the formation of $Mn(III)_2$ and Mn(II)Mn(III)-phenoxyl radical. The formation of Mn(II)Mn(III)-phenoxyl radical and $Mn(III)_2$ occurs at close potentials and are difficult to distinguish [39]. However, the growth of the relative intensity of the second oxidation wave with increasing scan rate suggests it corresponds to the ligand-centered oxidation to generate a Mn(II)Mn(III)-phenoxyl radical [40]. In the case of complex **7**, three non-reversible anodic processes are detected at $E_{pa1} \approx 0.4$ V, $E_{pa2} \approx 0.52$ V and $E_{pa3} \approx 0.79$ V vs *SCE* (Fig. S3(d)), which might be attributed to the formation of higher oxidation state complexes with concomitant formation of oxo-bridges. It must be observed that while reduction and first oxidation processes of **6** take place at potentials differing in 0.38 V, **7** shows electrochemical stability over ΔE = 0.56 V. Therefore, the introduction of carboxylate instead of the non-coordinating benzyl group in the ligand framework plays a significant role in the stabilization of the mixed valence Mn(II)Mn(III) state in dry DMF. An still larger ΔE (0.965 V) was reported for another triply phenolate-bis(acetate)-bridged Mn(II)Mn(III) complex where the benzyl group is replaced by pyridine, a donor stronger than carboxylate, with redox processes taking place at E_{red} = −0.057 V and E_{ox} = 0.908 V vs *SCE* in MeCN [19].

3.3. Catalase activity studies

3.3.1. Kinetics

In the previous sections it was shown that the replacement of the non-coordinating benzyl arm by the carboxylate in the ligand influences both the ligand-field splitting and the redox potentials. Thus, it is expected that this ligand changes also affect the catalase activity of the resulting complexes. The ability of complexes **6** and **7** to catalyze H_2O_2 disproportion was tested in DMF, CH_3CN, and CH_3OH. For both complexes, an immediate vigorous evolution of dioxygen was observed after addition of H_2O_2 to a solution of the catalyst. Turnovers as high as 3600 without significant decomposition were measured for the two complexes in DMF, and up to 600 and 300 equivalents of H_2O_2 were decomposed in CH_3CN and CH_3OH, respectively. Besides, in the last two solvents, the rate of O_2 evolution diminished after successive additions of H_2O_2. It is likely that the bridging ligands of the complexes serve as internal bases facilitating deprotonation of the peroxide coupled to the redox reaction. Therefore, in DMF, a non protic solvent (α_{DMF} = 0) [41], these catalysts disproportionate H_2O_2 with only slight loss of activity (Fig. S4). However, in the protic CH_3OH solvent (α_{MeOH} = 0.93) or CH_3CN, a solvent with intermediate proton donor ability (α_{MeCN} = 0.19), protonation of the bridges could inactivate the catalyst resulting in moderate to low turnover numbers. Therefore, DMF was chosen as solvent for evaluation of catalase activity.

The initial rate of H_2O_2 disproportionation by complexes **6** and **7** in DMF was measured as a function of the complex (Fig. S5) and substrate concentrations at 25 °C. As shown in Fig. 3, for both complexes, at constant $[H_2O_2]_0$ = 148 mM, the initial rate (r_i) varies linearly with the [catalyst], and the first-order rate constants k_1^6 = 24.5(3) min^{-1} and k_1^7 = 51.2(2) min^{-1} were obtained from the slope of the straight line.

At constant [catalyst] = 0.25 mM, complexes **6** and **7** exhibit saturation kinetics with $[H_2O_2]_0$ (Fig. 3) and the r_i/[catalyst] vs $[H_2O_2]_0$ data could be fitted to the Michaelis-Menten equation (Eq. (1)). In this equation, k_{cat} is the catalytic rate constant (turnover number) and K_M is a measure of the complex affinity for H_2O_2 (the lower the K_M value, the

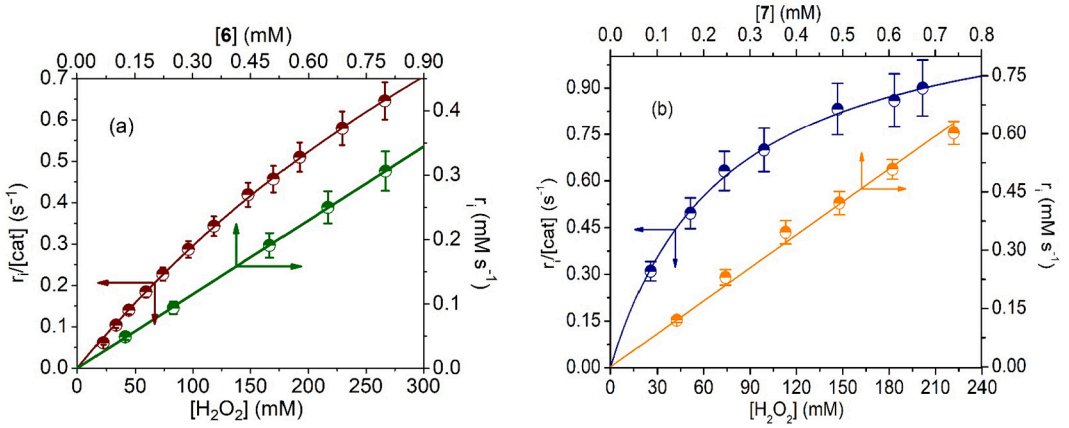

Fig. 3. Effect of $[catalyst]_0$ (green and orange lines; $[H_2O_2]$ = 148 mM) and $[H_2O_2]_0$ (brown and blue lines; [catalyst] = 0.25 mM) on the initial rate of H_2O_2 disproportionation catalyzed by (a) **6** and (b) **7** at 298 K, in DMF.

higher affinity for H_2O_2).

The values of catalytic turnover numbers $k^6_{cat} = 2.3(1)\ s^{-1}$ and $k^7_{cat} = 1.22(2)\ s^{-1}$, and Michaelis constants $K^6_M = 6.8(4) \times 10^{-1}$ M and $K^7_M = 7.3(5) \times 10^{-2}$ M, were determined from the non-linear fit of experimental data to Eq. 1 (solid wine and blue lines in Fig. 3).

$$\frac{r_i}{[\text{catalyst}]} = \frac{k_{cat}\,[H_2O_2]}{K_M + [H_2O_2]} \quad (1)$$

Kinetics results show that electron transfer between **6** and H_2O_2 is more effective (larger k_{cat}) than for **7**, but **6** is 10-times less efficient at binding the substrate ($K^6_M > K^7_M$), so that can reach a maximal rate ($V_{max} = k_{cat}$ [catalyst]) at $[H_2O_2]$ much higher than **7**. Based on the k_{cat}/K_M criterion, $\frac{k^6_{cat}}{K^6_M} = 3.38\ M^{-1}\ s^{-1}$ and $\frac{k^7_{cat}}{K^7_M} = 16.7\ M^{-1}\ s^{-1}$, the catalytic efficiency of **7** is ≈ 5-times higher than for complex **6**. The higher efficiency of **7** to disproportionate H_2O_2 is related to its larger affinity for binding peroxide, probably because the presence of the terminal carboxylate facilitates H_2O_2 binding through hydrogen bonding favoring the formation of the catalyst-H_2O_2 adduct [18,42].

3.3.2. *Spectroscopic monitoring of the catalase reaction*

In order to get insight into the mechanism of the H_2O_2 disproportionation catalyzed by complexes **6** and **7** in DMF, the reaction was monitored by using a combination of electronic and EPR spectroscopies and ESI-MS. UV–visible absorption spectra taken in DMF during the progress of the reaction of complex **6** with excess H_2O_2 exhibited an increase of the absorption band at 275 nm concurrently with the decrease of the absorbance at 365 nm (Fig. 4(a)) with an isosbestic point at 322 nm. The intensity of bands at longer wavelengths changed slightly during the reaction. The same spectral changes were observed upon successive additions of 100 equiv. of H_2O_2 to the DMF solution of the catalyst, and the O_2 production rate measured after each new addition was essentially constant, suggesting that the catalyst is stable in these reaction conditions.

After addition of 100 equiv. of H_2O_2 to a solution of **6** in DMF, the low-temperature X-band EPR spectra exhibit a broad signal (Fig. 4(a), inset) consistent with a weakly coupled Mn(II)Mn(III) center [17] overlapped to a six-line signal centered at $g = 2$ with hyperfine splitting of ≈ 93 G. This 6-line signal departs from that of the solvated Mn^{2+} ion and is characteristic of a Mn(II) center bound to the ligand that could arise from a Mn(III)Mn(II) species where the phenolate-bridge disrupted through protonation [36,37]. This cleavage of the phenolate bridge makes the diMn unit appear as the individual ions: an EPR silent Mn(III) and a mononuclear Mn(II) with a six-line signature. This was confirmed by addition of *p*-toluensulphonic acid to the solution of **6** in DMF giving the same EPR spectrum. This spectral pattern was kept at the end of the reaction. Retention of the complex nuclearity during the reaction was confirmed by mass spectrometry. ESI-mass spectra obtained after addition of 100 equiv. H_2O_2 to a DMF solution of **6** showed the parent peak at *m/z* 811.2 and other peaks already appearing in the spectrum of the starting solution and a new peak at *m/z* 773.2 corresponding to $[Mn_2L^1(OAc)(HCO_2)(OH)]^+$ (Fig. S6(a)), thus providing a clear indication that the diMn complex persisted during the catalytic cycle.

During the spectrophotometric monitoring of the reaction of **7** with excess H_2O_2 in DMF, the intensity of the *CT* band at 345 nm decreased

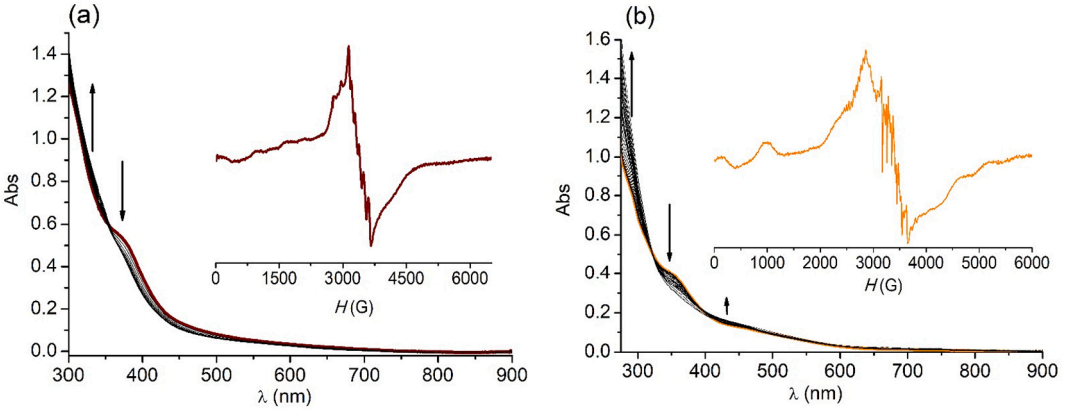

Fig. 4. UV–vis spectra of (a) **6** (0.125 mM) and (b) **7** (0.1 mM) after addition of 100 equiv. of H_2O_2, in DMF. T = 25 °C. Inset: X-band EPR spectra of 1 mM catalyst +100 equiv. H_2O_2 a few minutes after mixing. ν = 9.5 GHz, T = 110 K, microwave power = 0.5 mW.

and absorbance at 279 nm grew up, with an isosbestic point at 323 nm (Fig. 4(b)). Interestingly, the intensity of the band at 462 nm (PhO-to-dπ Mn(III) *CT*) also raised, although in a lesser proportion. These spectral changes suggest a different arrangement of phenolate groups around Mn(III) during catalysis. For this complex, the initial intensity of the *LMCT* bands was not restored at the end of the H_2O_2 disproportionation reaction. The EPR spectra taken during the **7** + H_2O_2 reaction course (Fig. 4(b), inset) showed broad lines expanded over the whole spectral range characteristic of diMn(II) species with weak anti-ferromagnetic exchange interactions [37,43,44] which originate from the contribution of the populated paramagnetic higher excited spin states [45]. Several sets of 11 lines are observed on the top of some of the more intense signals (i.e. signal centered at 2870 G), with an average hyperfine splitting of ≈ 43 G typical of the interaction between the electronic spin and two Mn(II) nuclear spins ($I_{Mn} = 5/2$). This $Mn(II)_2$ spectrum is superimposed to a 6-line signal at g ≈ 2 that arises from a small fraction of monomeric aqueous Mn^{2+} (up to 5% at the end of the reaction). The final EPR spectrum of the reaction mixture was identical to those registered during the reaction meaning the formed $Mn(II)_2$ species persists in solution, in agreement with absorption spectra. The disproportionation of H_2O_2 catalyzed by **7** was also followed by ESI-MS. Besides the parent peak at *m/z* 755 and other peaks already present in the starting complex solution, another intense peak is observed at *m/z* = 619.1 that can be attributed to $[Mn_2L^2]^+$, thus confirming the retention of dinuclearity of the complex during catalysis (Fig. S6(b)).

3.3.3. *Mechanism of the CAT-like reaction of **6** and **7***

The two complexes catalyze H_2O_2 disproportionation with first order kinetics on [catalyst], rates are essentially constant upon successive additions of H_2O_2, and O_2 evolution occurs without a time-lag at the onset of the reaction, all suggesting these complexes are responsible for the disproportionation of H_2O_2. Based on spectroscopic results, both compounds retain their dinuclearity during catalysis but employ a different redox cycle for H_2O_2 disproportionation. From the EPR spectra, the mixed valence Mn(II)Mn(III) complex **6** is present in solution during the catalytic cycle either in the coupled $[Mn(II)(\mu\text{-PhO})Mn(III)]^+$ or uncoupled $[Mn(II)(PhOH)Mn(III)]^{2+}$ forms. A possible mechanism is presented in Scheme 2, including the equilibrium of the uncoupled/coupled diMn species of **6** (observed in the EPR spectra) and species present in the ESI-mass spectra. It is proposed that **6** is the active reduced form of the catalyst that reacts with H_2O_2 in the slow reductive half-reaction (turnover-limiting step). The observation of saturation kinetics with substrate indicates that a catalyst-peroxide adduct is formed at this step, probably by substitution of the labile solvent molecule bound to Mn(III), which upon O—O bond breaking yields the μ-oxo-Mn(III)Mn(IV) and water. This oxidized form of the complex reacts with another H_2O_2 molecule in a fast-oxidative half-reaction to afford O_2 and restores the starting complex closing the cycle. This oxidative half-reaction must be much faster than the reductive one, so that the μ-oxo-Mn(III)Mn(IV) is not observed by EPR.

For H_2O_2 disproportionation catalyzed by complex **7**, the observation of a coupled $Mn(II)_2$ species in the EPR spectra taken during and at the end of the reaction suggests a redox cycle involving $Mn(II)_2$ and $Mn(III)_2$ oxidation states, as proposed in Scheme 3.

According to this scheme, initial oxidation of the starting Mn(II)Mn(III) complex by H_2O_2 affords $Mn(III)_2(OAc)_{1(2)}(\mu\text{-O(H)})$ species (EPR silent) in a fast step. In this way, the starting complex should be a precursor of the active complex. A similar one-electron oxidation of a precursor phenolate-bridged diMn(II) complex has already been reported [36]. The H_2O_2 binding to the starting complex can take place through acetate-shift to yield the μ-hydroxo-$Mn(III)_2$ species, where terminally bound acetate can be further protonated and partially dissociates. The higher labilizing effect of $L^{2(3-)}$ compared to $L^{1(2-)}$ may favor acetate dissociation as evidenced by the high proportion of the Mn_2L^+ species in the mass spectra. The μ-oxo-$Mn(III)_2$ species is proposed to be the oxidized active form of the catalyst that enters the catalytic cycle of H_2O_2 dismutation. The absence of a lag-time at the onset of the reaction is consistent with the oxidation of the mixed valence complex being faster than the H_2O_2 disproportionation reaction. Hydrogen bond to the terminally bound carboxylate group of the ligand within the catalyst-H_2O_2 adduct (Fig. S7) may account for the higher efficiency of this complex for binding peroxide (low K_M value) which renders **7** more efficient to catalyze H_2O_2 disproportionation than **6**.

At pH 7, the electrochemical potentials for the two-electron O_2/H_2O_2 and H_2O_2/H_2O redox couples are +0.04 V and +1.11 V vs *SCE*, respectively. If disproportionation of H_2O_2 occurs through an outer-sphere mechanism, only diMn complexes with redox couples between the H_2O_2 reduction and oxidation potentials should be active. However, a number of complexes that exhibit redox potentials outside the H_2O_2 dismutation range react efficiently [7,14], suggesting diMn complexes dismutate H_2O_2 through an inner-sphere mechanism with electron transfer taking place within the catalyst-peroxide adduct, in agreement with the saturation kinetics observed for a number of diMn mimics. In Table 1, the catalytic efficiency (k_{cat}/K_M values) of complexes **6** and **7** is

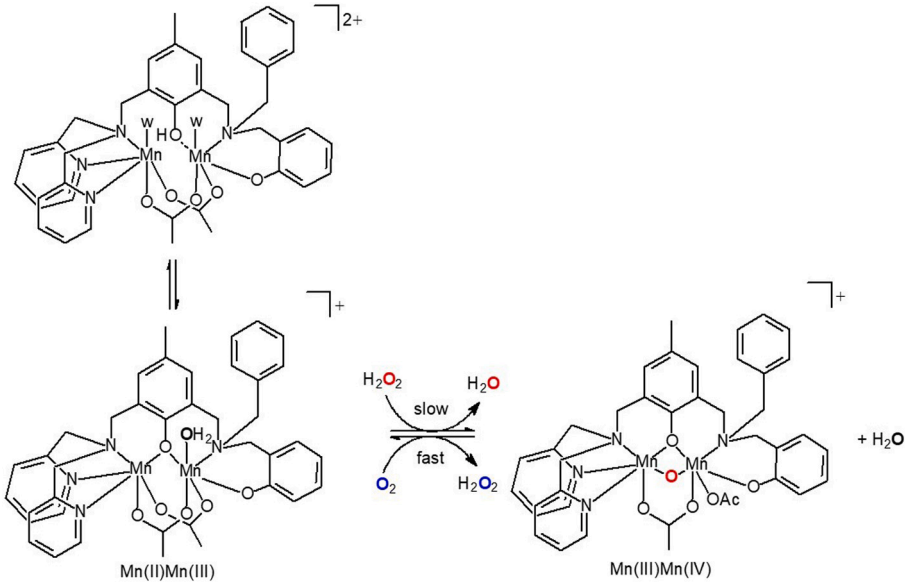

Scheme 2. Proposed catalytic cycle for complex **6**.

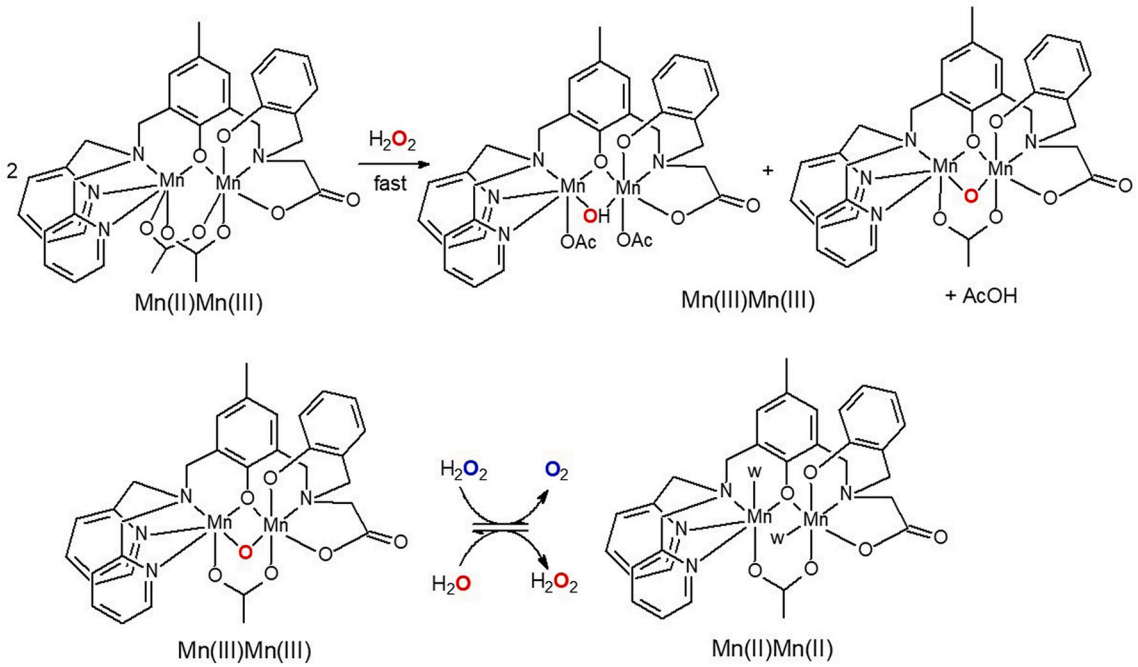

Scheme 3. Proposed catalytic cycle for complex **7**.

Table 1
Catalytic efficiency of phenolate-bridged diMn complexes for disproportionating H_2O_2.

	Complex	k_{cat}/K_M or k (M^{-1} s^{-1})	Bridging ligands	Ligand terminal groups	Redox cycle	Mn···Mn (Å)	Refs
1	**7**	16.7	(μ-phO)(μ-OAc)$_2$	py$_2$/phO$^-$,CO$_2^-$	Mn(II)$_2$/Mn(III)$_2$	–	This work
2	[Mn$_2$(bcpmp)(μ-OAc)$_2$]	11.44	(μ-phO)(μ-OAc)$_2$	py,CO$_2^-$/py,CO$_2^-$	Mn(II)Mn(III)/Mn(II*I*)Mn(IV)	3.47	[17]
3	[Mn$_2$L(OH)$_2$(H$_2$O)$_2$]	5.08[a]	(μ-phO)	(CO$_2^-$)$_2$/(CO$_2^-$)$_2$	Mn(II)$_2$/Mn(III)$_2$	3.67[d]	[18]
4	[Mn$_2$(bphpmp)(μ-OAc)$_2$(H$_2$O)]$^+$	4.7[b]	(μ-phO)(μ-OAc)$_2$	py$_2$/py,phO$^-$	NR	3.497	[19]
5	[Mn$_2$(bpbp)(μ-OAc)$_2$]$^{2+}$	3.76	(μ-phO)(μ-OAc)$_2$	py$_2$/py$_2$	Mn(II)Mn(III)/Mn(II*I*)Mn(IV)	3.45	[17,46]
6	**6**	3.38	(μ-phO)(μ-OAc)$_2$	py$_2$/phO$^-$	Mn(II)Mn(III)/Mn(II*I*)Mn(IV)	–	This work
7	[Mn$_2$(bphba)$_2$(Cl)$_2$]	1.1	(μ-phO)$_2$	py$_2$/py$_2$	Mn(II)$_2$/Mn(III)$_2$	3.41	[47,48]
8	[Mn$_2$(HBPClNOL)(BPClNOL)Cl]$^+$	80.2[c]	(μ-phO)(μ-OR)	py,RO$^-$/py,phO$^-$	Mn(II)Mn(III)/Mn(II*I*)Mn(IV)	3.16	[30]
9	[Mn$_2$(μ-OMe)(OAc)(hppentO)]$^+$	106.3	(μ-OR)$_2$(μ-OAc)	py,phO$^-$/py,phO$^-$	Mn(II)$_2$/Mn(III)$_2$	2.95	[49]
10	MnCAT (*T. thermophilus*)	3.1×10^6	(μ-OH)(μ-OH$_2$)(μ-OAc)	His,Glu/His,Glu,H$_2$O	Mn(II)$_2$/Mn(III)$_2$	3.18; 3.03	[50,51,13]

NR = not reported. Bcpmp = 2,6-bis({(carboxymethyl)[(1-pyridyl)methyl]amino}methyl)-4-methylphenol]; bpbp = 2,6-bis{[bis(2-pyridylmethyl)amino]methyl}-4-tert-butylphenol; bphba = 2-{(*N*,*N*-bis(2-pyridylmethyl)amino)methyl}phenol; bphpmp = 2-[bis(2-pyridylmethyl)aminomethyl]-6-{[(2-hydroxybenzyl)(2-pyridylmethyl)amino]methyl}-4-methylphenol; LH_4 = 5-methyl-2-hydroxo-1,3-xylene-α,α-diamine-N,N,N′,N′-tetraacetic acid; H_2BPClNOL = N-(2-hydroxybenzyl)-N-(2-pyridylmethyl)[(3-chloro)(2-hydroxy)]propylamine; H_2hppentOH = 1,5-Bis[(2-hydroxybenzyl)(2-pyridylmethyl)amino]pentan-3-ol.

[a] Second-order kinetics.
[b] Calculated from reported data.
[c] In the presence of piperazine, pH 9.7.
[d] Calculated from an optimized geometry.

compared to other phenolate-bridged diMn complexes of ligands with different terminal N/O donors that employ either Mn(II)$_2$/Mn(III)$_2$ or Mn(II)Mn(III)/Mn(III)Mn(IV) redox cycles during catalysis. For those complexes with low affinity for the substrate (large K_M value) that do not achieve saturation with [H_2O_2], second-order rate constants (k_{2cat}) are given for comparison, considering that when $K_M \gg [H_2O_2]$, the denominator of Eq. 1 is dominated by K_M, and $r_i = \frac{k_{cat}}{K_M}$ [catalyst][H_2O_2] = k_{2cat} [catalyst][H_2O_2].

The catalytic efficiency of triply bridged (μ-phenolate)bis($\mu_{1,3}$-carboxylate)diMn complexes falls into two groups. Complexes bearing terminal carboxylate that react with efficiency higher than 11 M^{-1} s^{-1} (entries 1–2), and those with pyridyl/phenolate arms that react with efficiency lower than 5 M^{-1} s^{-1} (entries 4–6), highlighting the role of carboxylate to facilitate the formation of the adduct with H_2O_2 through hydrogen bond. Phenolate-bridged [Mn$_2$L(OH)$_2$(H$_2$O)$_2$] with no acetate bridges but four carboxylate arms, is placed in between these two groups, with the carboxylate groups compensating the long intermetallic separation that disfavors the cooperativity between the two Mn ions for the electron transfer process (entry 3). Bis(μ-phO)diMn complexes are even less efficient than any of the (μ-phenolate)bis($\mu_{1,3}$-carboxylate) diMn complexes, one example is shown in entry 7. Enhanced activity is observed when the two Mn ions are linked by one or two alcoholate bridges (entries 8–9) where the intermetallic distance is shorter than in the phenolate-bridged complexes. As can be observed in Table 1, the

Mn···Mn separation in phenolate-bridged complexes is longer than 3.4 Å, while in the (μ-alcoholate)$_n$diMn complexes the Mn···Mn distance is closer to the value reported for the enzyme (3.03 and 3.18 Å for the oxidized and reduced forms, respectively, entry 10), strengthening the cooperativity between the two Mn ions.

4. Conclusions

Unsymmetrical N_4O_2-hexadentate H_2L^1 and N_4O_3-heptadentate NaH_2L^2 ligands afford mixed valence Mn(II)Mn(III) complexes **6** and **7** where each Mn ion is in a different coordination environment. Both complexes share the coordination sphere of the Mn(II) ion, but differ in the donor groups surrounding Mn(III). In **6**, the sixth coordination position of Mn(III) is occupied by a water molecule, while in **7** Mn(III) is bound to the NO_3-donor sites of the ligand and two additional O-atoms from bridging acetates, leaving this metal ion coordinatively saturated. The replacement of the non-coordinating benzyl arm of L^1 by the carboxylate arm in L^2 modifies the ligand field splitting, the reduction potential and the reactivity of the resulting complex. Therefore, complex **7** catalyzes H_2O_2 disproportionation more efficiently than **6**, even when the formation of the catalyst-peroxide adduct must take place through acetate-shift in **7** but by direct replacement of a labile solvent molecule in **6**. This different reactivity can be interpreted in terms of the larger affinity of **7** for the substrate (smaller K_M value), attributed to the ability of the terminal carboxylate group of the ligand to stabilize the adduct through hydrogen bond to H_2O_2, and to the higher labilizing effect of the heptadentate ligand that favors the acetate-shift. These two combined effects in **7** render $K_M = 0.073$ M, that compares well to $K_M = 0.083$ M of MnCAT of *T. thermophilus* [50], and, based on the k_{cat}/K_M criterion, place complex **7** as the most efficient among the phenolate-bridged diMn catalysts. Given that acetate-shift is also an initial process in the phosphohydrolase activity [52], further catalytic studies of complexes **6** and **7** as hydrolase mimics will be undertaken to test the bifunctionality of these complexes.

Declaration of competing interest

The authors declare that they have no known competing financial interests or personal relationships that could have appeared to influence the work reported in this paper.

Acknowledgments

This work was supported by the National University of Rosario (PIP-BIO553) and the Consejo Nacional de Investigaciones Científicas y Técnicas (CONICET, PIP 0337 and PUE 0068), the Centre National de la Recherche Scientifique (CNRS, PICS 07121), and the Agency for Science, Technology and Innovation of Santa Fe (ASACTeI, IO 2010-164-16). R. Mehrotra thanks CONICET for a post-doctoral fellowship.

Appendix A. Supplementary data

Supplementary data to this article can be found online at https://doi.org/10.1016/j.jinorgbio.2020.111264.

References

[1] B. Yang, Y. Chen, J. Shi, Chem. Rev. 119 (2019) 4881–4985.
[2] J.E. Penner-Hahn, in: V.L. Pecoraro (Ed.), Manganese Redox Enzymes, VCH, New York, 1992.
[3] D. Salvemini, C. Muscoli, D.P. Riley, S. Cuzzocrea, Pulm. Pharmacol. Ther. 15 (2002) 439–447.
[4] J.M. McCord, M.A. Edeas, Biomed. Pharmacother. 59 (2005) 139–142.
[5] A. Mahammed, Z. Gross, Catal. Sci. Technol. 1 (2011) 535–540.
[6] C. Policar, in: J.S. Reboucas, I. Batinic-Haberle, I. Spasojevic, D.S. Warner, D. St. Clair (Eds.), Redox Active Therapeutics, Springer, Berlin, 2016, pp. 125–164.
[7] S. Signorella, C. Palopoli, G. Ledesma, Coord. Chem. Rev. 365 (2018) 75–102.
[8] Y. Ning, Y. Huo, H. Xue, Y. Du, Y. Yao, A.C. Sedgwick, H. Lin, C. Li, S.-D. Jiang, B.-W. Wang, S. Gao, L. Kang, J.L. Sessler, J.-L. Zhang, J. Am. Chem. Soc. 142 (2020) 10219–10227.
[9] P.J. Riggs-Gelasco, R. Mei, J.E. Penner-Hahn, H.H. Thorp, V.L. Pecoraro (Eds.), Mechanistic Bioinorganic Chemistry, American Chemical Society, Washington, DC, 1995 (Chapter 8).
[10] W.C. Stallings, K.A. Pattridge, R.A. Strong, M.L. Ludwig, J. Biol. Chem. 260 (1985) 16424–16432.
[11] S. Signorella, C. Palopoli, V. Daier, G. Ledesma, R.H. Kretsinger, E.A. Permyakov, V.N. Uversky (Eds.), Encyclopedia of Metalloproteins, Springer, New York, 2013, pp. 1283–1292.
[12] V.V. Barynin, M.M. Whittaker, S.V. Antonyuk, V.S. Lamzin, P.M. Harrison, P. J. Artymyuk, J.M. Whittaker, Structure 9 (2001) 725–738.
[13] S.V. Antonyuk, W.R. Melik-Adamiyan, V.R. Popov, V.S. Lamzin, P.D. Hempstead, P.M. Harrison, P.J. Artymiuk, V.V. Barynin, Crystallogr. Rep. 45 (2000) 105–116.
[14] S. Signorella, C. Hureau, Coord. Chem. Rev. 256 (2012) 1229–1245.
[15] A.J. Wu, J.E. Penner-Hahn, V.L. Pecoraro, Chem. Rev. 104 (2004) 903–938.
[16] S. Abdolahzadeh, J.W. de Boer, W.R. Browne, Eur. J. Inorg. Chem. (2015) 3432–3456.
[17] R. Singh, M. Haukka, C.J. McKenzie, E. Nordlander, Eur. J. Inorg. Chem. (2015) 3485–3492.
[18] V. Solís, C. Palopoli, V. Daier, E. Rivière, F. Collin, D. Moreno, C. Hureau, S. Signorella, J. Inorg. Biochem. 182 (2018) 29–36.
[19] P. Karsten, A. Neves, A.J. Bertoluzzi, J. Strahle, C. Maichle-Mossmer, Inorg. Chem. Commun. 5 (2002) 434–438.
[20] L. Dubois, R. Caspar, L. Jacquamet, P.-E. Petit, M.-F. Charlot, C. Baffert, M.-N. Collomb, A. Deronzier, J.-M. Latour, Inorg. Chem. 42 (2003) 4817–4827.
[21] G.N. Ledesma, E. Anxolabéhère-Mallart, L. Sabater, C. Hureau, S.R. Signorella, J. Inorg. Biochem. 186 (2018) 10–16.
[22] A. Neves, M.A. de Brito, V. Drago, K. Griesar, W. Haase, Inorg. Chim. Acta 237 (1995) 134–135.
[23] E. Lambert, B. Chabut, S. Chardon-Noblat, A. Deronzier, G. Chottard, A. Bousseksou, J.-P. Tuchagues, J. Laugier, M. Bardet, J.-M. Latour, J. Am. Chem. Soc. 119 (1997) 9424–9437.
[24] L.L. Koh, J.O. Ranford, W.T. Robinson, J.O. Svensson, A.L.C. Tan, D. Wu, Inorg. Chem. 35 (1996) 6466–6472.
[25] C. Belle, G. Gellon, C. Scheer, J.L. Pierre, Tetrahedron Lett. 35 (1994) 7019–7022.
[26] R.N. Salvatore, C.H. Yoon, K.W. Jung, Tetrahedron 57 (2001) 7785–7811.
[27] B. Capon, W.G. Overend, M. Sobell, Tetrahedron (16) (1961) 106–112.
[28] C. Palopoli, G. Gómez, A. Foi, F. Doctorovich, S. Mallet-Ladeira, C. Hureau, S. Signorella, J. Inorg. Biochem. 167 (2017) 49–59.
[29] A. Gelasco, M.L. Kirk, J.W. Kampf, V.L. Pecoraro, Inorg. Chem. 36 (1997) 1829–1837.
[30] R.O. Costa, S.S. Ferreira, C.A. Pereira, J.R. Harmer, C.J. Noble, G. Schenk, R.W. A. Franco, J.A.L.C. Resende, P. Comba, A.E. Roberts, C. Fernandes, A. Horn Jr., Front. Chem. 6 (2018) 491, https://doi.org/10.3389/fchem.2018.00491.
[31] R. Lomoth, P. Huang, J. Zheng, L. Sun, L. Hammarström, B. Akermark, S. Styring, Eur. J. Inorg. Chem. (2002) 2965–2974.
[32] C. Hureau, L. Sabater, F. Gonnet, G. Blain, J. Sainton, E. Anxolabéhère-Mallart, Inorg. Chim. Acta 359 (2006) 339–345.
[33] M.M. Whittaker, C.A. Ekberg, R.A. Edwards, E.N. Baker, G.B. Jameson, J. W. Whittaker, J. Phys. Chem. B 102 (1998) 4668–4677.
[34] H. Diril, H.-R. Chang, M.J. Nilges, X. Zhang, J.A. Potenza, H.J. Schugar, S.S. Isied, D.N. Hendrickson, J. Am. Chem. Soc. 111 (1989) 5102–5114.
[35] M.G. Patch, K.P. Simolo, C.J. Carrano, Inorg. Chem. 21 (1982) 2972–2977.
[36] L. Dubois, D.-F. Xiang, X.-S. Tan, J.-M. Latour, Eur. J. Inorg. Chem. (2005) 1565–1571.
[37] L. Dubois, D.-F. Xiang, X.-S. Tan, J. Pécaut, P. Jones, S. Baudron, L. Le Pape, J.-M. Latour, C. Baffert, S. Chardon-Noblat, M.-N. Collomb, A. Deronzier, Inorg. Chem. 42 (2003) 750–760.
[38] A.E.M. Boelrijk, G.C. Dismukes, Inorg. Chem. 39 (2000) 3020–3028.
[39] T. Kurahashi, A. Kikuchi, T. Tosha, Y. Shiro, T. Kitagawa, H. Fujii, Inorg. Chem. 47 (2008) 1674–1686.
[40] T.K. Paine, T. Weyhermüller, E. Bothe, K. Weighardt, P. Chandhuri, Dalton Trans. (2003) 3136–3144.
[41] J. Shorter, Correlation Analysis of Organic Reactivity, Research Studies Press, New York, 1983, pp. 146–153.
[42] L. Dubois, J. Pecaut, M.-F. Charlot, C. Baffert, M.-N. Collomb, A. Deronzier, J.-M. Latour, Chem. Eur. J. 14 (2008) 3013–3025.
[43] C. Hureau, L. Sabater, E. Anxolabéhère-Mallart, M. Nierlich, M.-F. Charlot, F. Gonnet, E. Rivière, G. Blondin, Chem. Eur. J. 10 (2004) 1998–2010.
[44] C. Hureau, S. Blanchard, M. Nierlich, G. Blain, E. Rivière, J.-J. Girerd, E. Anxolabéhère-Mallart, G. Blondin, Inorg. Chem. 43 (2004) 4415–4426.
[45] S. Blanchard, G. Blain, Eric Rivière, M. Nierlich, G. Blondin, Chem. Eur. J. 9 (2003) 4260–4268.
[46] Y. Gultneh, Y.T. Tesema, T.B. Yisgedu, R.J. Butcher, G. Wang, G.T. Yee, Inorg. Chem. 45 (2006) 3023–3033.
[47] N. Reddig, D. Pursche, M. Kloskowski, C. Slinn, S.M. Baldeau, A. Rompel, Eur. J. Inorg. Chem. (2004) 879–887.
[48] S. Signorella, A. Rompel, K. Büldt-Karentzopoulos, B. Krebs, V.L. Pecoraro, J.-P. Tuchagues, Inorg. Chem. 46 (2007) 10864–10868.
[49] H. Biava, C. Palopoli, C. Duhayon, J.-P. Tuchagues, S. Signorella, Inorg. Chem. 48 (2009) 3205–3214.

[50] M. Shank, V. Barynin, G. Dismukes, Biochemistry 33 (1994) 15433–15436.
[51] V.V. Barynin, P.D. Hempstead, A.A. Vagin, S.V. Antonyuk, W.R. Melik-Adamyan, V.S. Lamzin, P.M. Harrison, P.J. Artymiuk, J. Inorg. Biochem. 67 (1997) 196.
[52] S.J. Smith, M.J. Riley, C.J. Noble, G.R. Hanson, R. Stranger, V. Jayaratne, G. Cavigliasso, G. Schenk, L.R. Gahan, Inorg. Chem. 48 (2009) 10036–10048.